Supporting information for

Elastic phase-change fibers with thermal energy storage based on a tunable TPU aerogel network constructed via a universal ambient pressure drying strategy

Yunyan Zhu[a,b], Jiatong Yan[a,b], Weijie Wang[a,b], Chuanxi Lin[a,b], Shouxiang Jiang[c], Hong Tang[d], Ronghui Guo[a,b*]

a. College of Biomass Science and Engineering, Sichuan University, Chengdu 610065, China
b. Ministry Education Key Lab Leather Chemistry & Engineering, Sichuan University, Chengdu 610065, Sichuan, China
c. School of Fashion and Textiles, The Hong Kong Polytechnic University, Kowloon, Hong Kong, 999077, China
d. Materials Science and Engineering, College of Design and Engineering, National University of Singapore Blk EA, #03-09 9 Engineering Drive 1 Singapore 117575

Content

~~1. Experimental Section~~

*Corresponding Author. Ronghui Guo, E-mail address: ronghuiguo214@126.com

Fabrication of different kinds of aerogel fibers (AFs) via BSR-APD strategy

Fabrication of meta-aramid AF. 1.0 g LiCl was added into 20.0 g N, N-Dimethylformamide (DMF) and stirred for dissolution at 80 °C. 1.4 g meta-aramid was then dissolved into the solution at 120 °C to obtain the 7% meta-aramid spinning solution after removal of the air bubbles by centrifuging at 3000 rpm for 20 min. Subsequently, meta-aramid spinning solution was extruded from a needle (19G, 740 μm) with a constant flow rate (0.25 mL min^{-1}) into deionized water coagulation bath to form meta-aramid wet fiber using wet spinning technology. Finally, 7% meta-aramid AF was obtained after binary solvents (TBA and n- hexane) replacement with ambient pressure drying (BSR-APD) strategy.

Fabrication of Kevlar aramid nanofiber AF. Kevlar aramid chopped fibers were added to 70% ethanol solution, ultrasonically washed for 1 h, and then washed with water several times, and then dried in an oven at 105°C. 2.5 g Kevlar aramid fibers and 2.5 g potassium tertbutoxide were added into a mixed solution with 97.5 mL DMSO and 2.5 g anhydrous methanol as cosolvents, and rapidly stirred for 8 h at room temperature to form a dark red spinning solution. The 2.5% Kevlar aramid nanofiber spinning solution was extruded from a needle (19G, 740 μm) with a constant flow rate (1.1 mm min^{-1}) into deionized water coagulation bath to form Kevlar aramid hydrogel fiber using wet spinning technology. Subsequently, 2.5% Kevlar aramid nanofiber AF was obtained via the BSR-APD strategy.

Fabrication of cellulose acetate AF. 1.0 g LiCl was added into 20.0 g N, N-Dimethylacetamide (DMAc) and stirred for dissolution at 55 °C. 3 g cellulose acetate was then dissolved into the solution to obtain the 15% cellulose acetate spinning solution after removal of the air bubbles by centrifuging at 3000 rpm for 20 min. Subsequently, the cellulose acetate spinning solution was extruded from a needle (19G, 740 μm) with a constant flow rate (0.25 mL min^{-1}) into deionized water coagulation bath to form cellulose acetate wet fiber using wet spinning technology. Subsequently, 15% cellulose acetate AF was obtained via the BSR-APD strategy.

Fabrication of TPU/MXene composite AF. The aqueous MXene dispersion was prepared by selectively etching Ti_3AlC_2 with LiF/HCl solvent system in accordance with our previous study [1]. The aqueous MXene dispersion was then transferred into DMSO via a solvent exchange method using repeated centrifugation at 9000 rpm for 1 h. The MXene supernatant was removed and replaced with DMSO and the sediment was redispersed through manual shaking for three times to maximize water removal and obtain MXene dispersions in DMSO. Then, the MXene/TPU spinning solution with

MXene loadings of 10 wt% was prepared by dissolving TPU granules in MXene/DMSO dispersions using stirring. Subsequently, the MXene/TPU spinning solution was injected into a coagulation bath of 4% acetic acid aqueous solution with a constant flow rate (0.25 mL min^{-1}) through a needle (19G, 740 μm) using wet spinning technology. Subsequently, 15% TPU/MXene composite AF was obtained via the BSR-APD strategy.

Fabrication of PAN AF. 2.8 g PAN was dissolved into 20 g DMF at 60 ℃ to obtain 14% PAN spinning solution. Subsequently, the PAN spinning solution was extruded from a needle (19G, 740 μm) with a constant flow rate (0.25 mL min^{-1}) into deionized water coagulation bath to form PAN wet fiber using wet spinning technology. Subsequently, 14% PAN AF was obtained via the BSR-APD strategy.

2. Supporting Figures

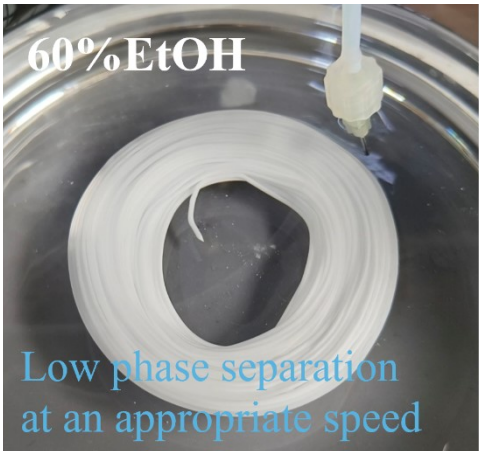

Fig. S1 Digital image of the TPU wet fibers formed by extruding 20% TPU/DMF spinning solution into 60%EtOH coagulation bath.

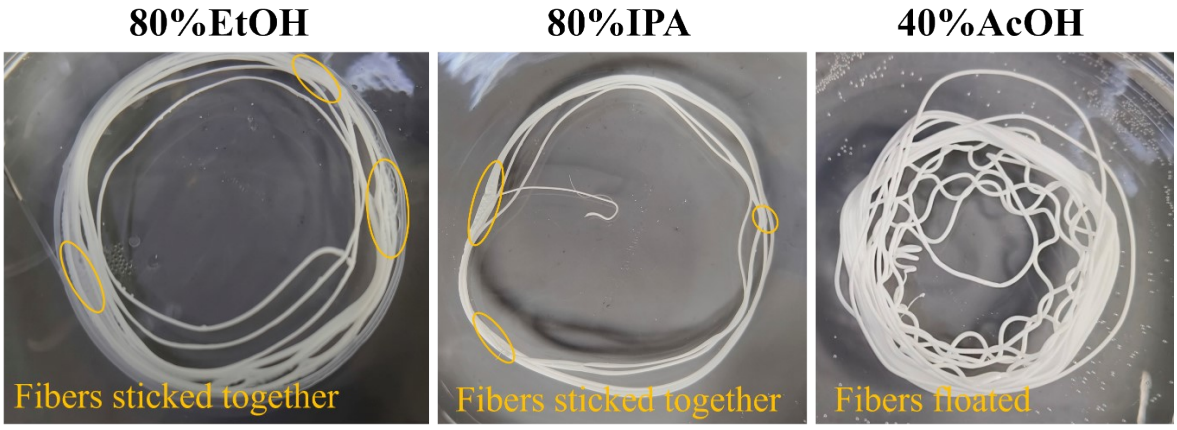

Fig. S2 Digital image of the TPU wet fibers formed by extruding 20% TPU/DMF spinning solution into coagulation baths with inappropriate ratios.

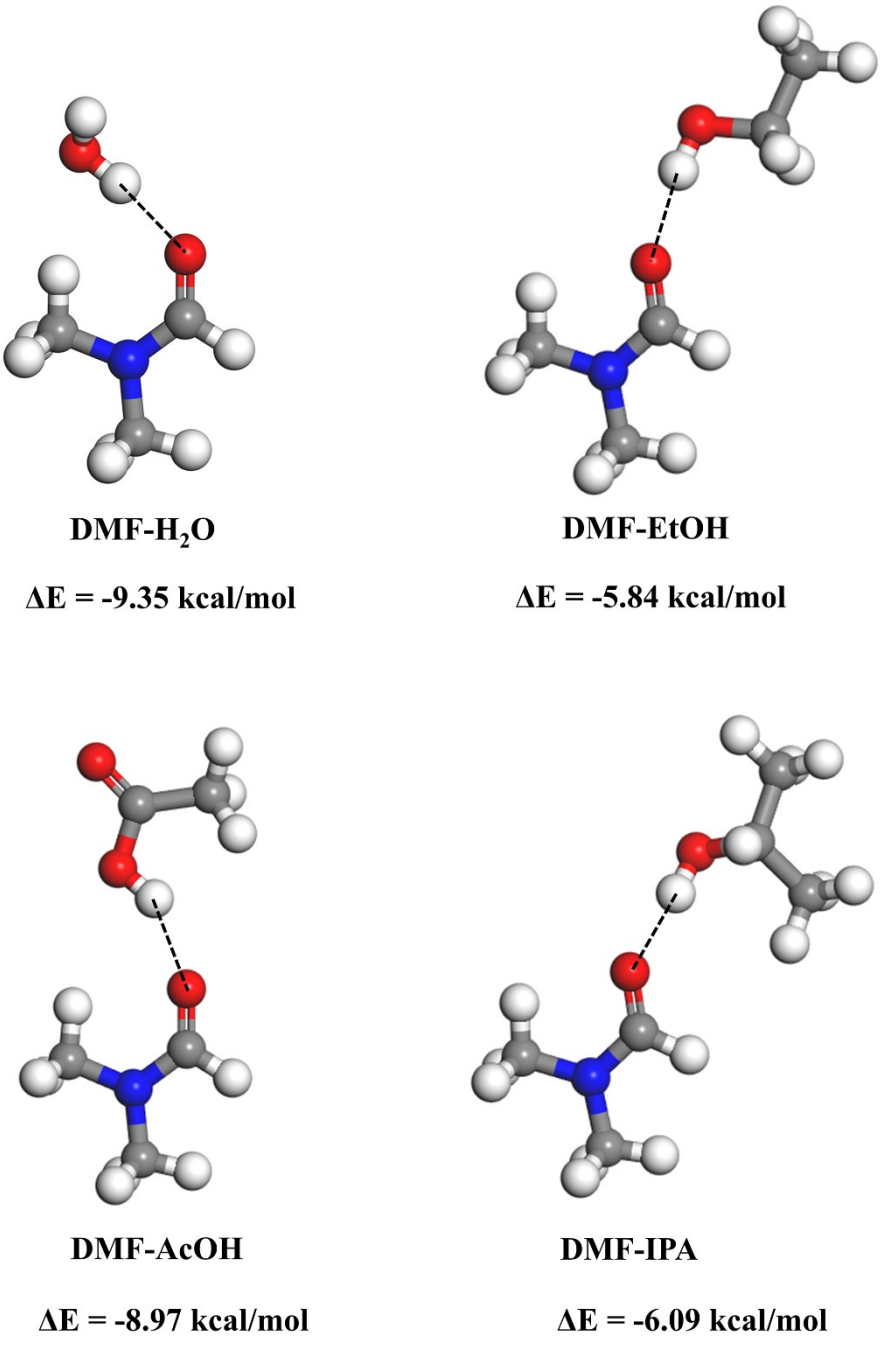

Fig. S3 Calculation values of hydrogen bonding energy of DMF-H_2O, DMF-EtOH, DMF-AcOH and DMF-IPA via theoretical simulation.

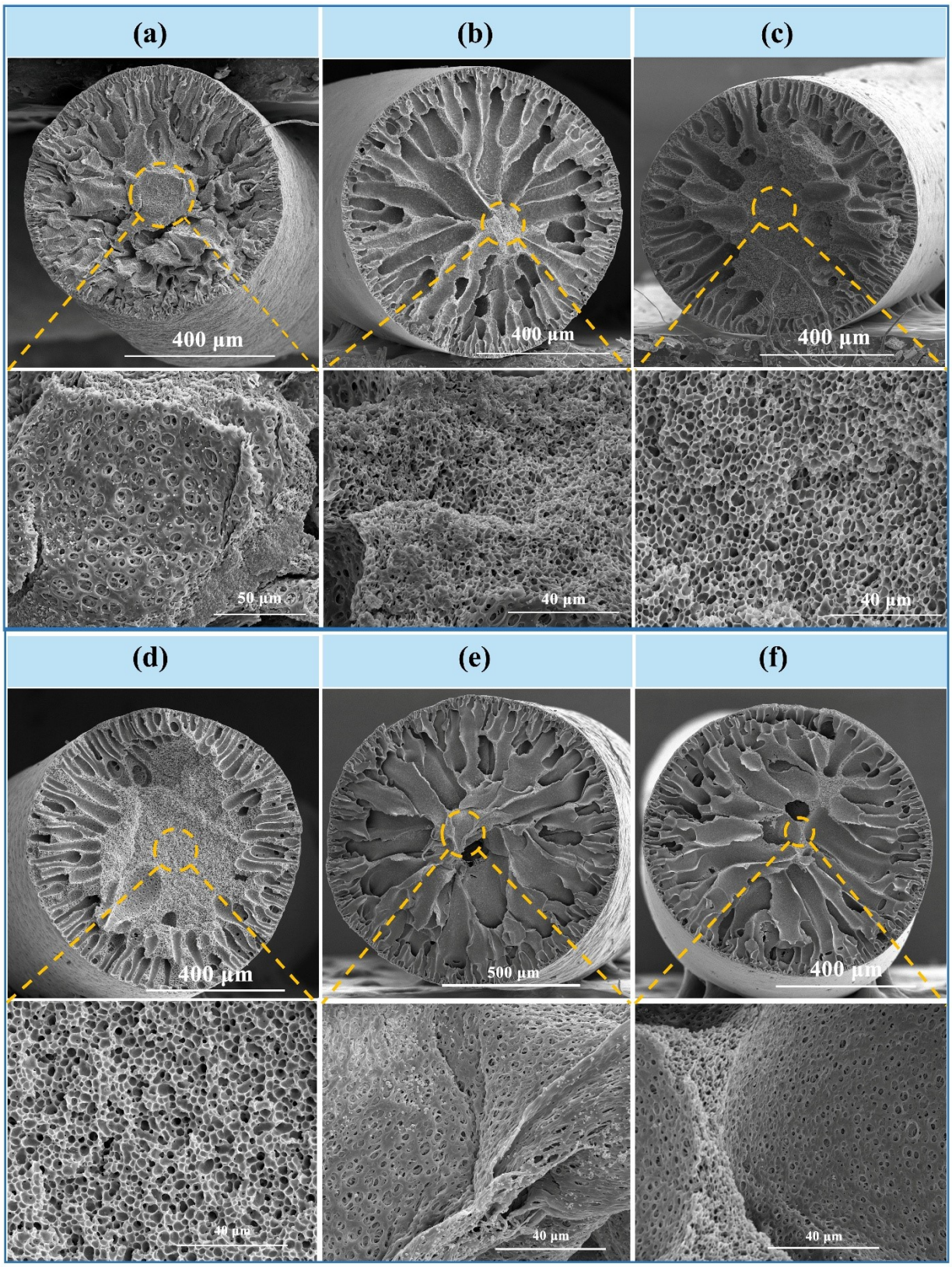

Fig. S4 SEM images of (a) 20%$TAF_{DMF\text{-}in\text{-}H_2O}$-APD, (b) 20%$TAF_{DMF\text{-}in\text{-}H_2O}$-FD, (c) 20%$TAF_{DMF\text{-}in\text{-}EtOH60}$-APD, (d) 20%$TAF_{DMF\text{-}in\text{-}EtOH60}$-FD, (e) 20%$TAF_{DMSO\text{-}in\text{-}H_2O}$-APD and (f) 20%$TAF_{DMSO\text{-}in\text{-}EtOH60}$-APD.

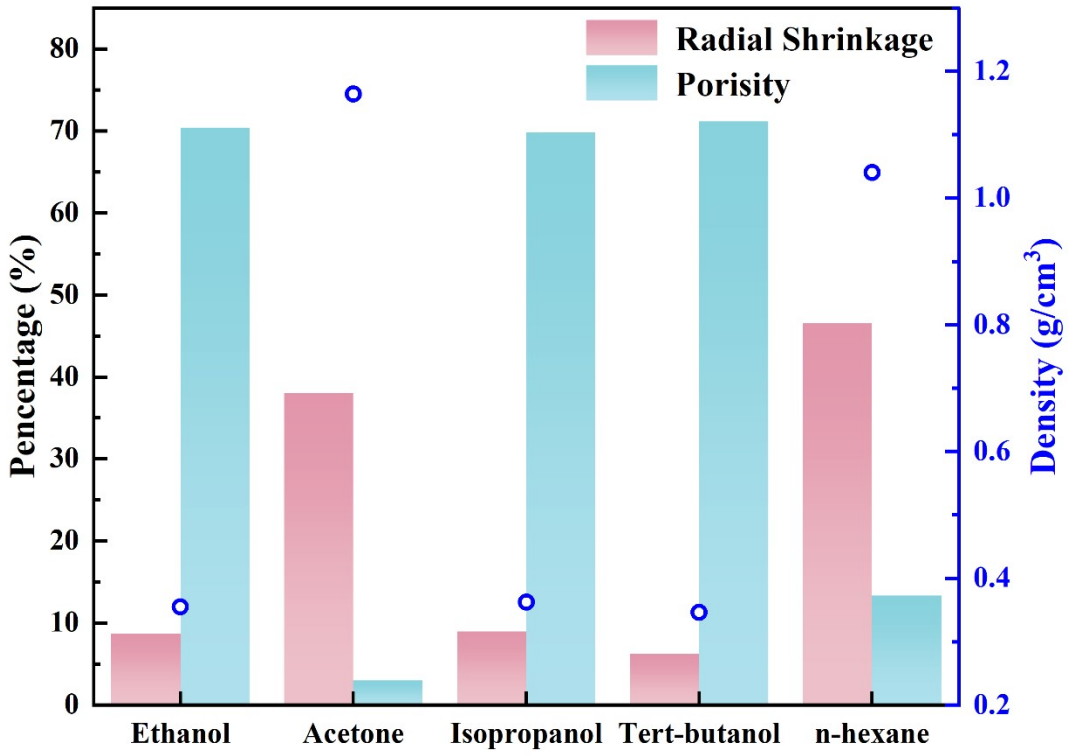

Fig. S5 The radial shrinkage, porosity and density of TPU fibers obtained by extruding 20% TPU/DMF spinning solution into 60%EtOH coagulation bath, followed by single solvent replacement and APD.

Lowering the surface tension effectively reduces capillary stress and suppresses structural shrinkage according to the Laplace equation ($\Delta P=2\gamma\cos\theta/r$). The surface tension of ethanol, isopropanol and Tert-butanol are much lower than that of water (72.81 mN/m) and no drastic structural shrinkage occurs due to high capillary stress during drying. TPU aerogel fiber with replacement by Tert-butanol had the lowest shrinkage rate among them. This can be attributed to the lower surface tension of Tert-butanol (20.30 mN/m) than those of ethanol (22.87 mN/m) and isopropanol (21.70 mN/m), resulting in lower capillary stress and thereby a more shrinkage reduction. Moreover, Tert-butanol has the weaker polarity compared with ethanol and isopropanol, and better compatibility with subsequent n-hexane. Thus, Tert-butanol is considered as the best intermediate replacement solvent. In contrast, adopting acetone replacement followed by APD cannot obtain TPU aerogel fiber. The use of acetone weakens the supporting strength of the TPU aerogel network because its rapid evaporation and partial

dissolving effect on TPU induce local swelling of the polymer chains. Thus, single solvent replacement with acetone easily leads to the collapse of the whole aerogel network and fiber shrinkage. And n-hexane alone failed to obtain TPU aerogel fiber with the presence of shrinkage and pore collapse during APD. Although n-hexane possesses extremely low surface tension (17.90 mN/m), its immiscibility with water leads to ineffective displacement and the residual water generates huge capillary pressure, destroying the TPU aerogel network structure. BSR-APD strategy can prevent shrinkage (2.51%) of the TPU aerogel network during APD stage through the synergistic two-step replacement of Tert-butanol and n-hexane, enabling BSR-APD as an efficient alternative to freeze-drying for obtaining TPU aerogel fibers.

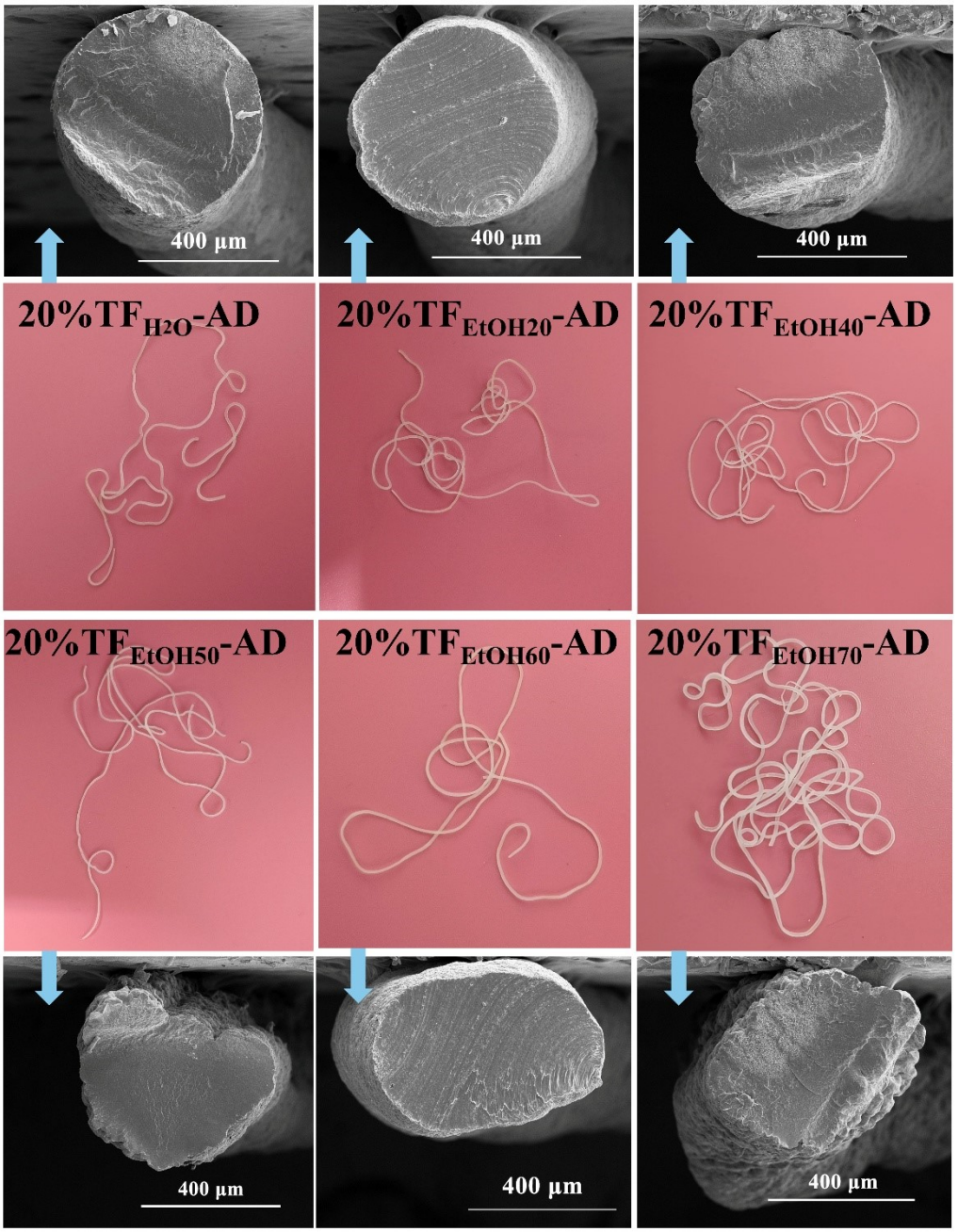

Fig. S6 Digital images and SEM images of the translucent TFs fibers formed by AD method.

Fig. S7 Optical microscope photos of TPU fibers (solid and porous states) formed into various volume ratios of EtOH coagulation bath before and after drying under different drying methods (AD, FD and APD).

(Note: The wet fibers are referred to the fibers through solvent-displaced twice with deionized water for comparison on the effects of different EtOH ratios on the macroscopic size and microscopic morphology of 20%TPU fibers.)

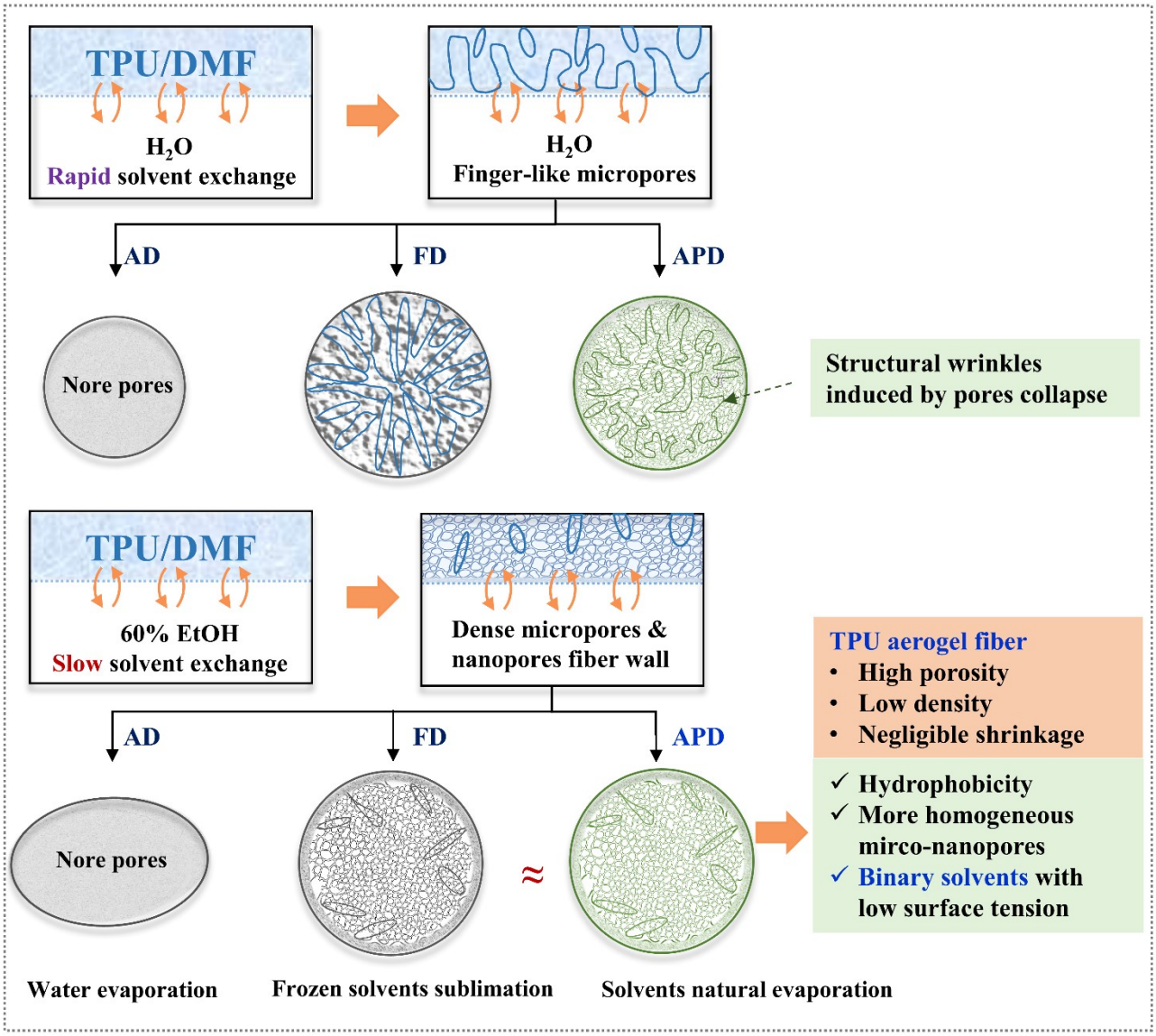

Fig. S8 Influence mechanisms of phase separation rates and different drying methods (AD, FD and APD) on the formation of TPU aerogel fibers.

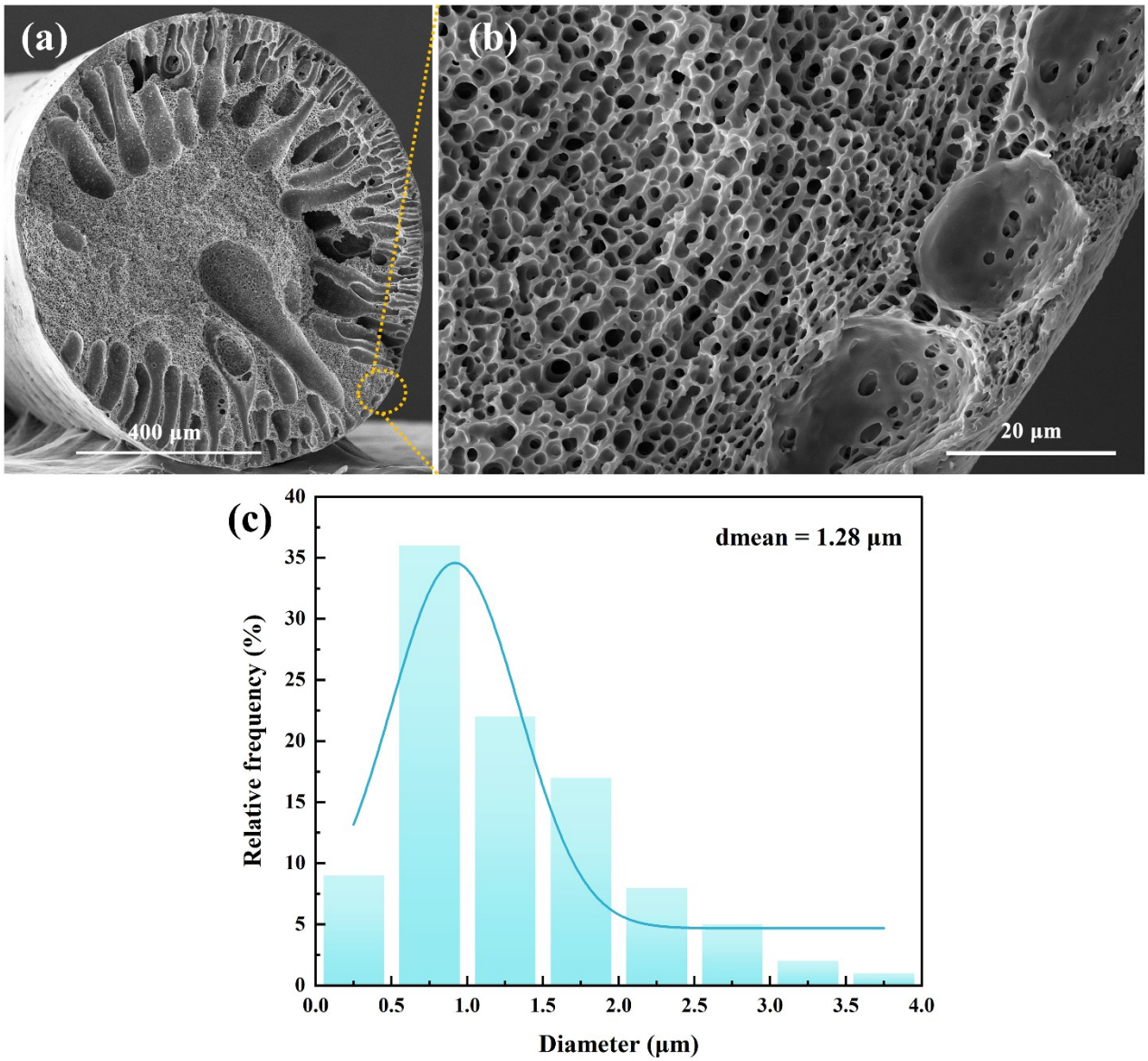

Fig. S9 SEM images and pore distribution of the thin fiber walls of the 20%TAF$_{EtOH60}$-APD with nanoporous structures formed under slow phase separation.

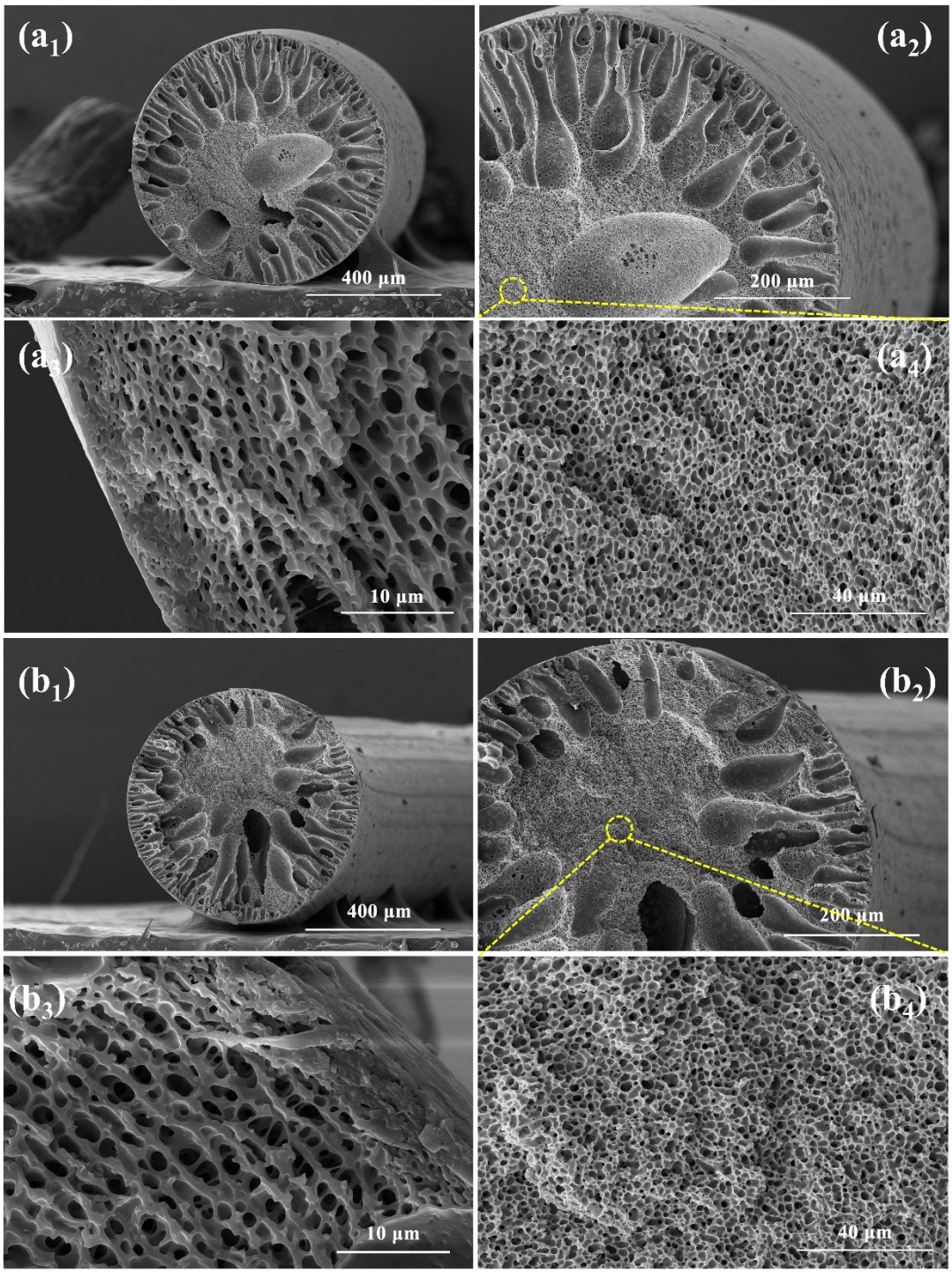

Fig. S10 SEM images of the 20%TAF_{EtOH60}-APD extruded with 20G needle (a_1-a_4) and 21G needle (b_1-b_4).

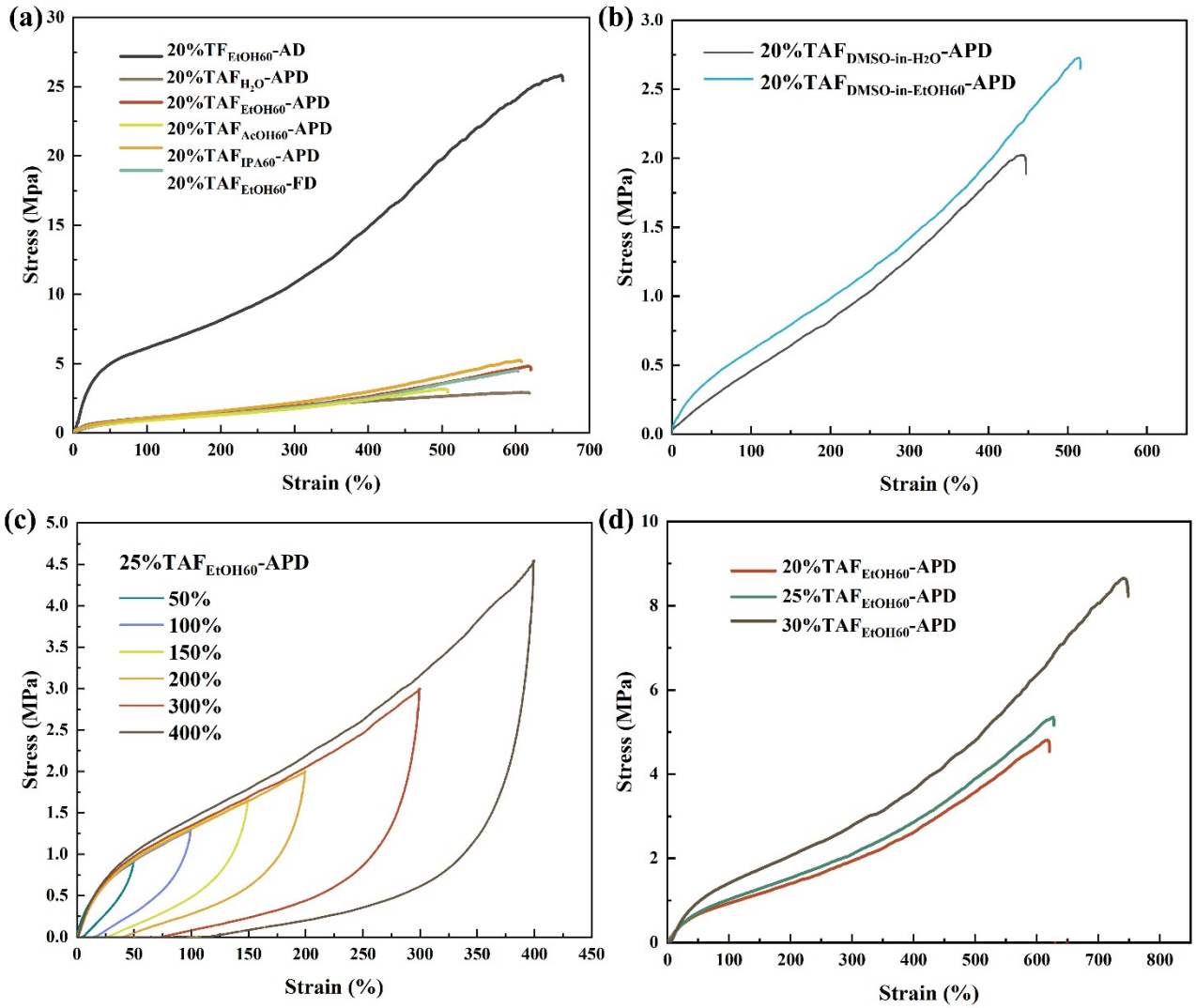

Fig. S11 Tensile stress-strain curves of TPU fibers (solid and porous). (a) Tensile stress-strain curves of TPU fibers (solid and porous) prepared with DMF as solvent by AD, APD and FD methods; (b) Tensile stress-strain curves of TAFs prepared with DMSO as solvent by APD method; (c) Stress-strain curves of 25%TAF$_{EtOH60}$-APD using DMF as solvent under different strains (50%, 100%, 150%, 200%, 300% and 400%); (d) Tensile stress-strain curves of TAFs with different spinning concentrations (20%, 25% and 30%) prepared with DMF as solvent by BSR-APD strategy.

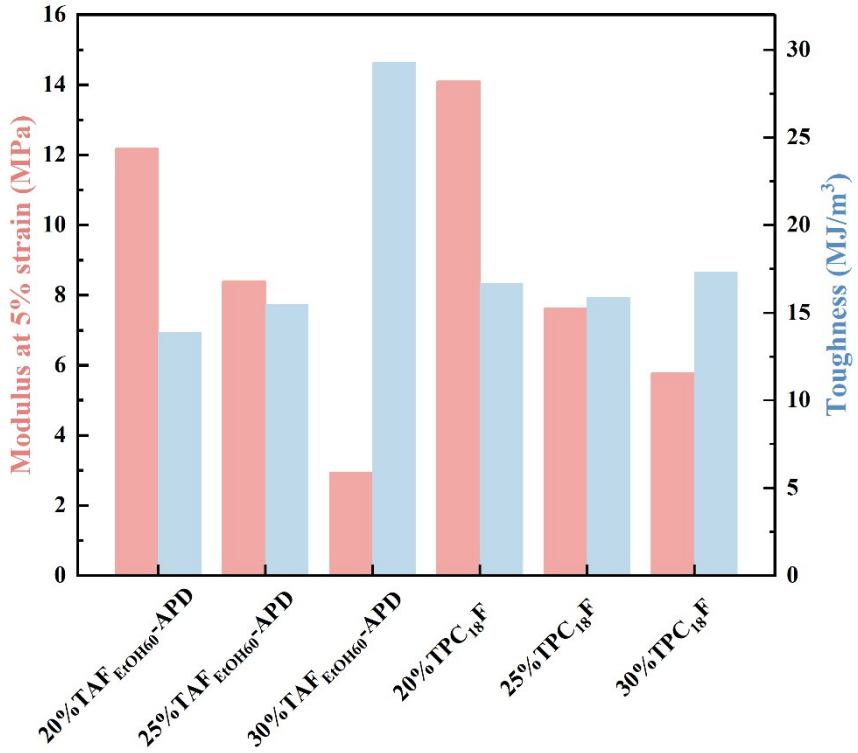

Fig. S12 Modulus at 5% strain and toughness of the TAFs prepared via BSR-APD method and the $TPC_{18}Fs$ prepared via vacuum impregnation of C18.

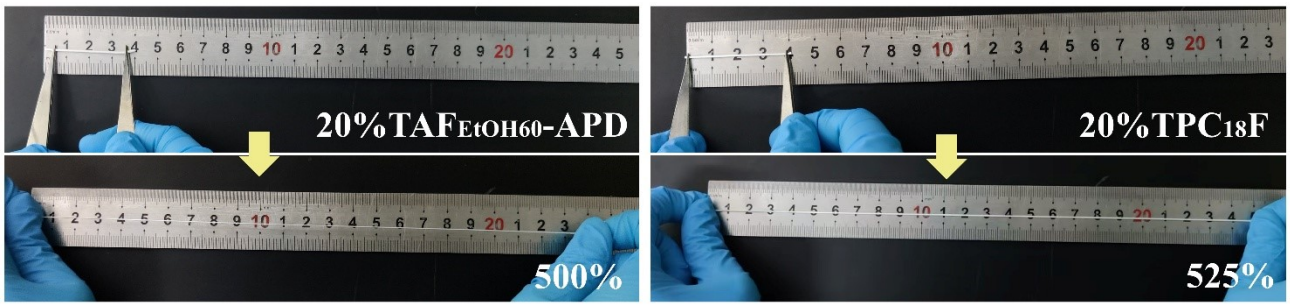

Fig. S13 Photograph of original state and stretched state of $20\%TAF_{EtOH60}$-APD and $20\%TPC_{18}F$.

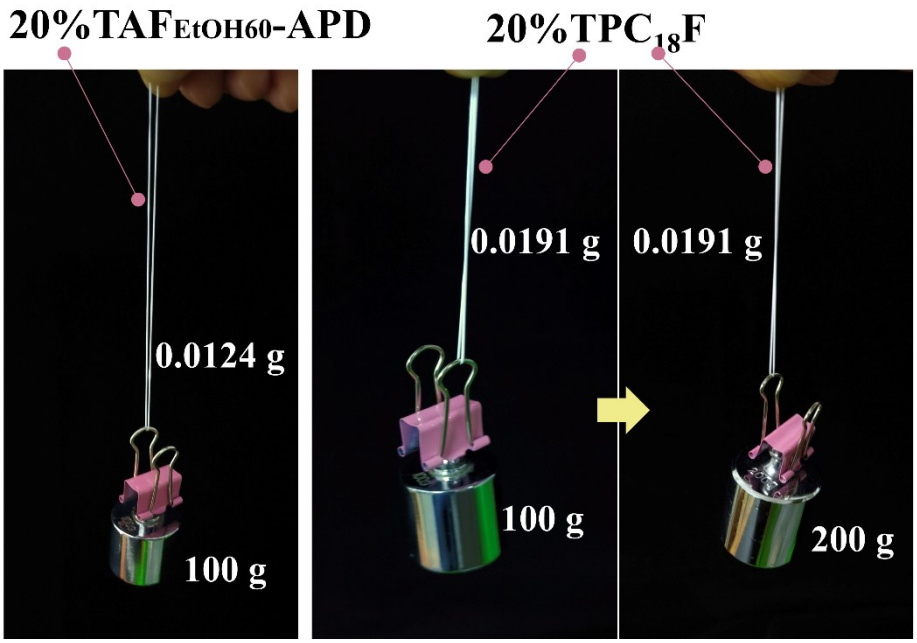

Fig. S14 Photograph of a single 20%TAF_{EtOH60}-APD under tensile load of 100 g and a single 20%$TPC_{18}F$ under tensile load of 100 g or 200 g.

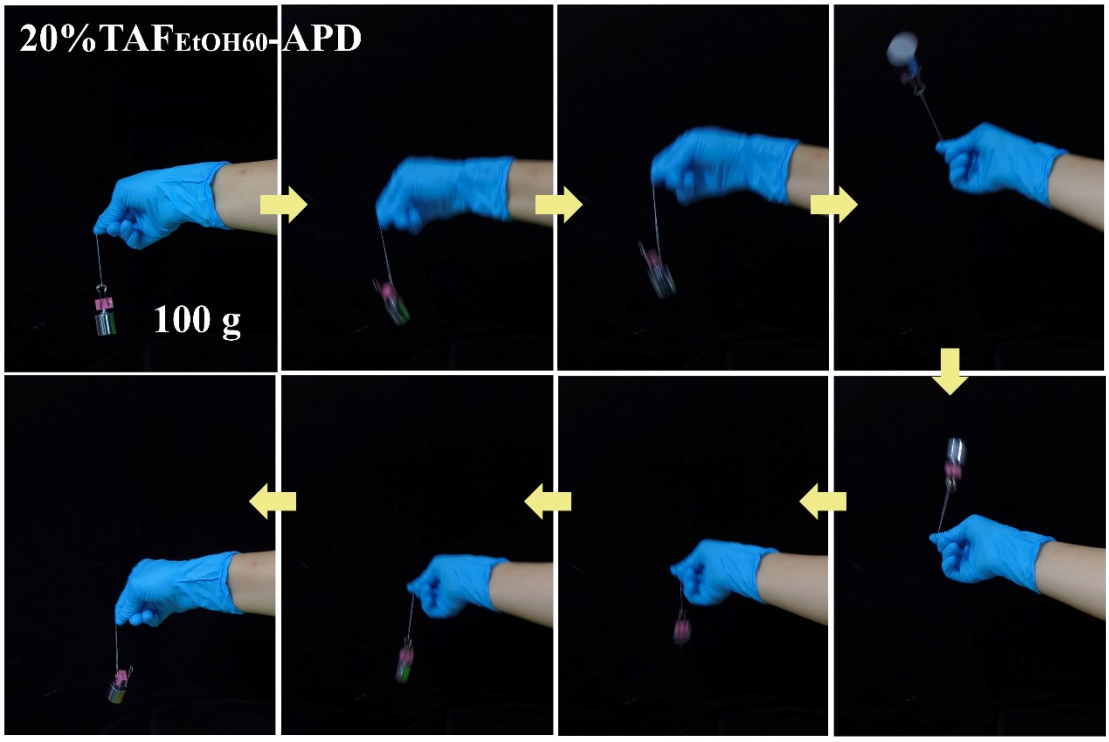

Fig. S15 Photograph of single 20%TAF_{EtOH60}-APD being loaded 100 g weights and swung at 360◦.

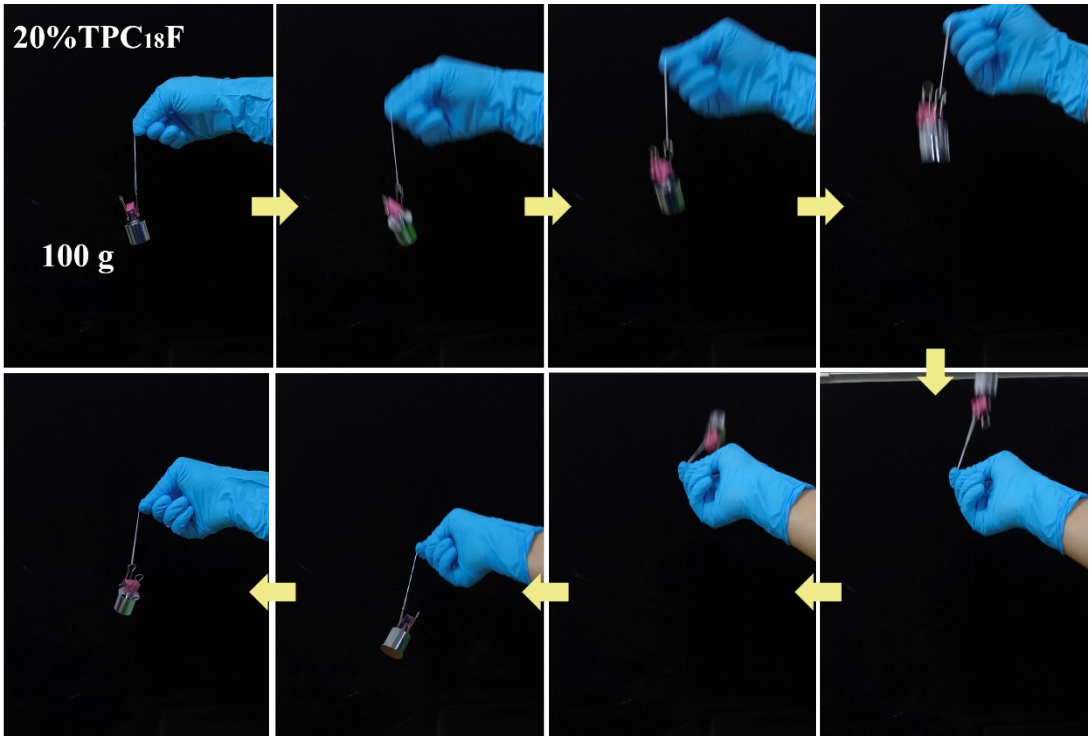

Fig. S16 Photograph of single 20%$TPC_{18}F$ being loaded 100 g weights and swung at 360◦.

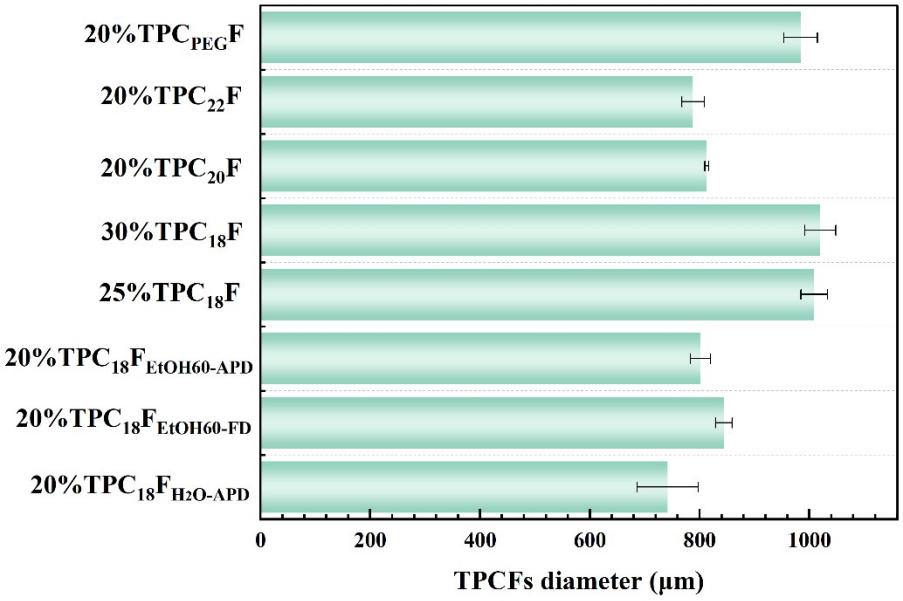

Fig. S17 Diameter of the TPCFs.

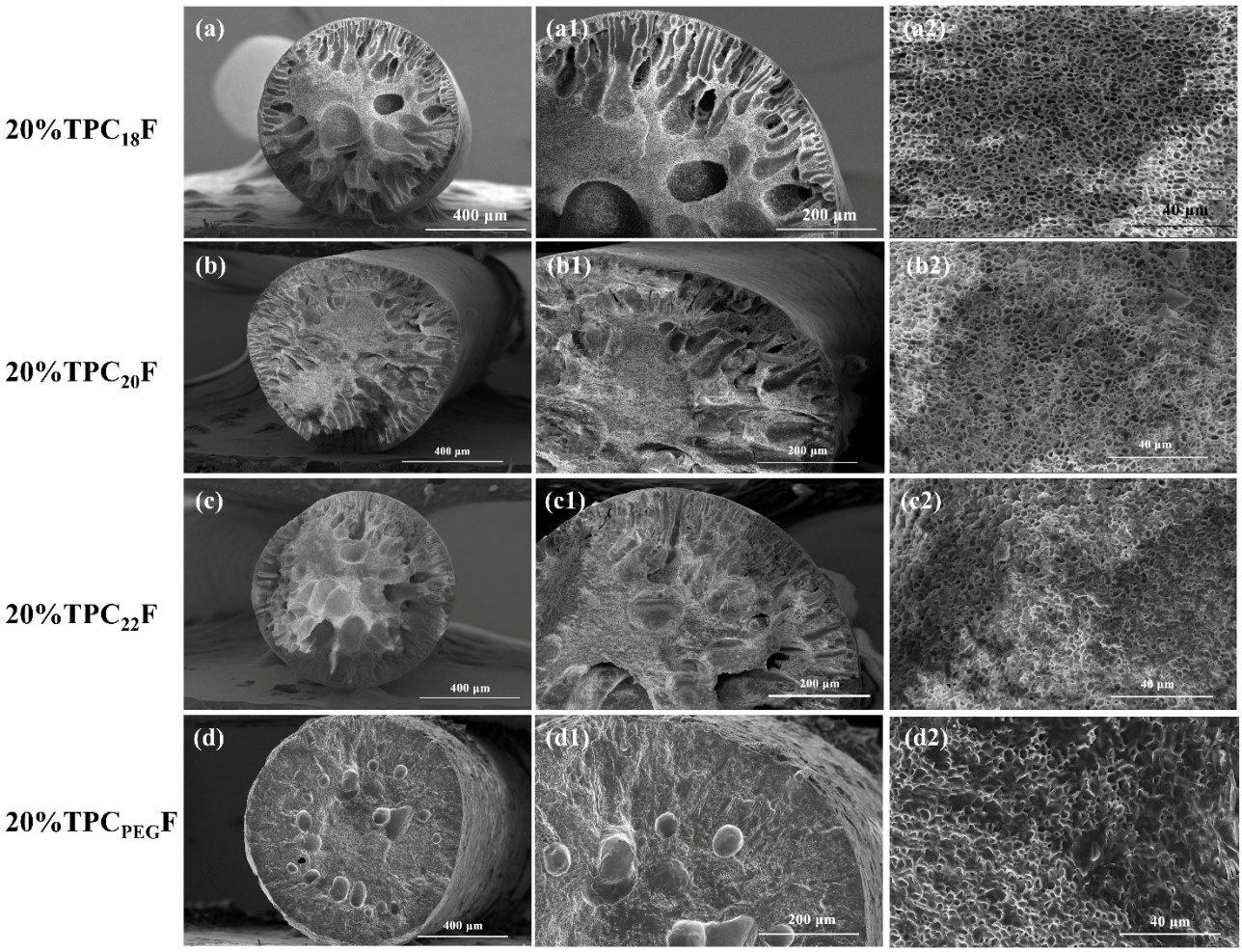

Fig. S18 SEM images of (a, a1, a2) 20%$TPC_{18}F$, (b, b1, b2) 20%$TPC_{20}F$, (c, c1, c2) 20%$TPC_{22}F$ and (d, d1, d2) 20%$TPC_{PEG}F$

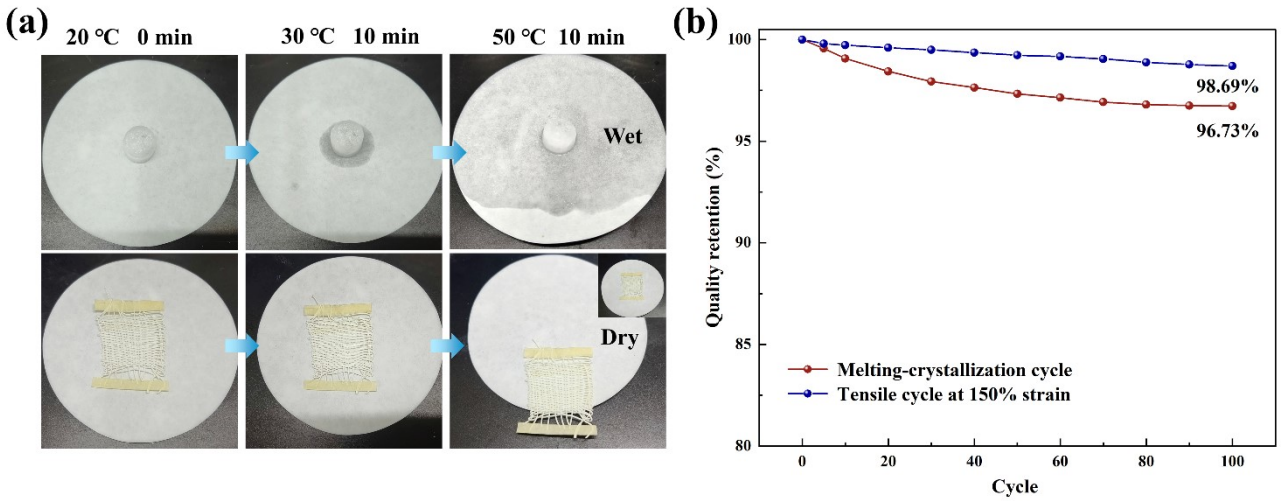

Fig. S19 Anti-leakage performance and leakage behavior of the samples: (a) digital images of C18 and TPC18F fabric during leakage tests and (b) quality retention of 20%TPC18F after repeated melting-crystallization cycles and tensile cycles at 150% strain.

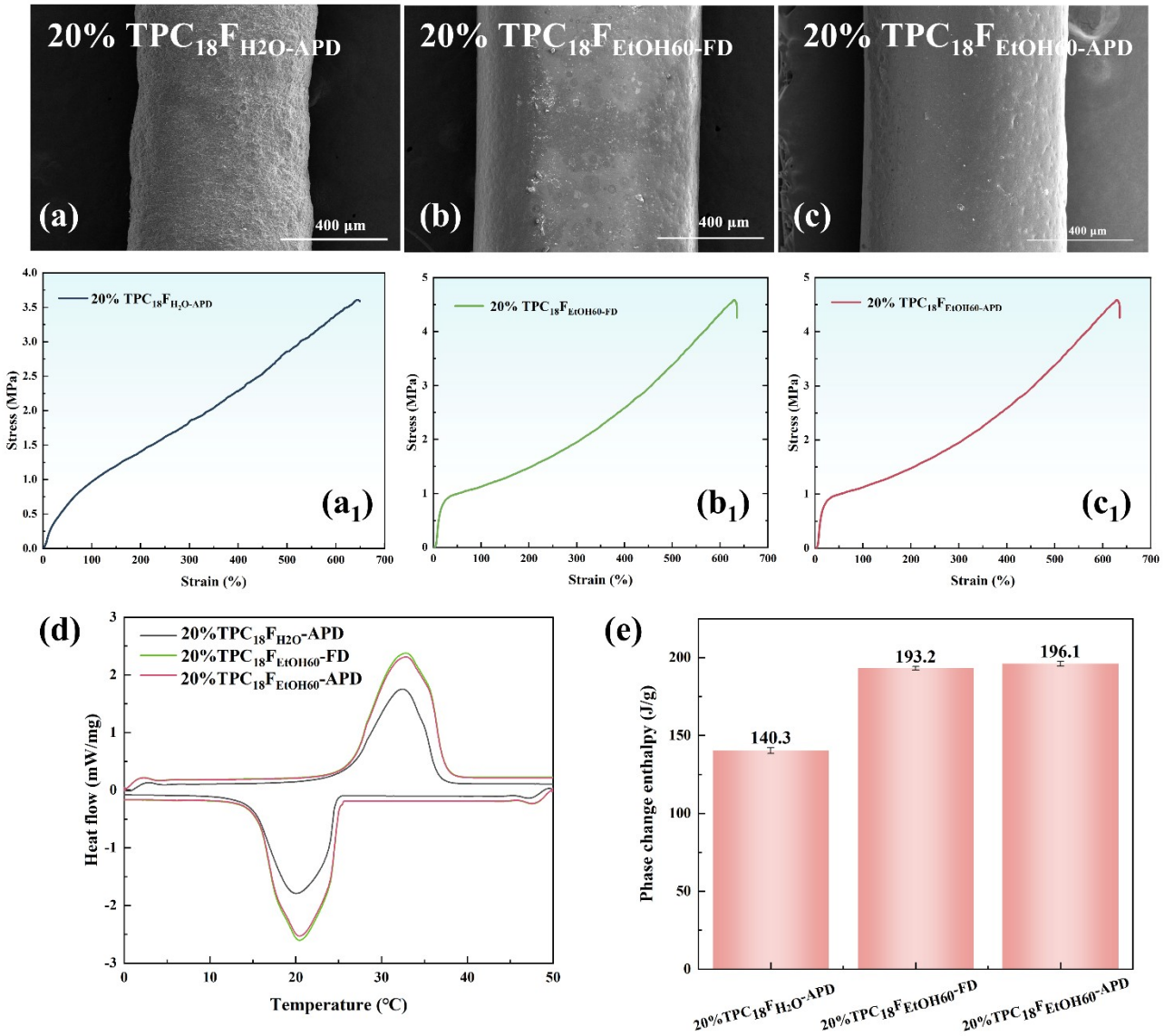

Fig. S20 Surface SEM images (a, b and c), tensile stress-strain curves (a_1, b_2 and c_2), DSC curves (d) and phase change enthalpy (e) of the 20%TPC_{18}Fs by vacuum impregnation of C18 into 20%TAF_{H2O}-APD, 20%TAF_{EtOH60}-FD and 20%TAF_{EtOH60}-APD.

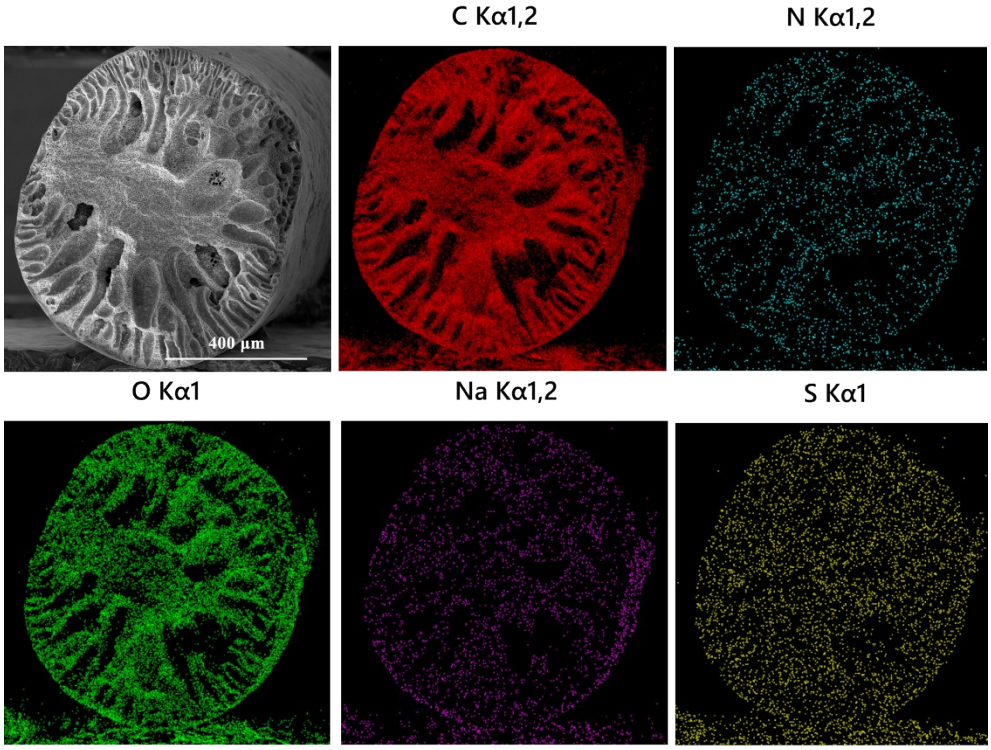

Fig. S21 SEM image and elemental mapping images of the 20%$TPC_{18}F$-Red by EDS.

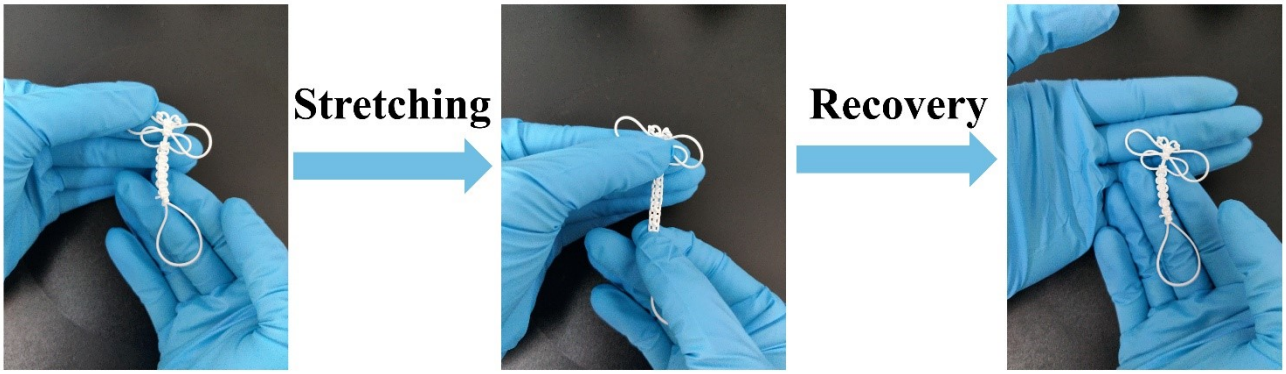

Fig. S22 Mechanical stretching and recovery behavior of a hand-woven white dragonfly using $TPC_{18}F$.

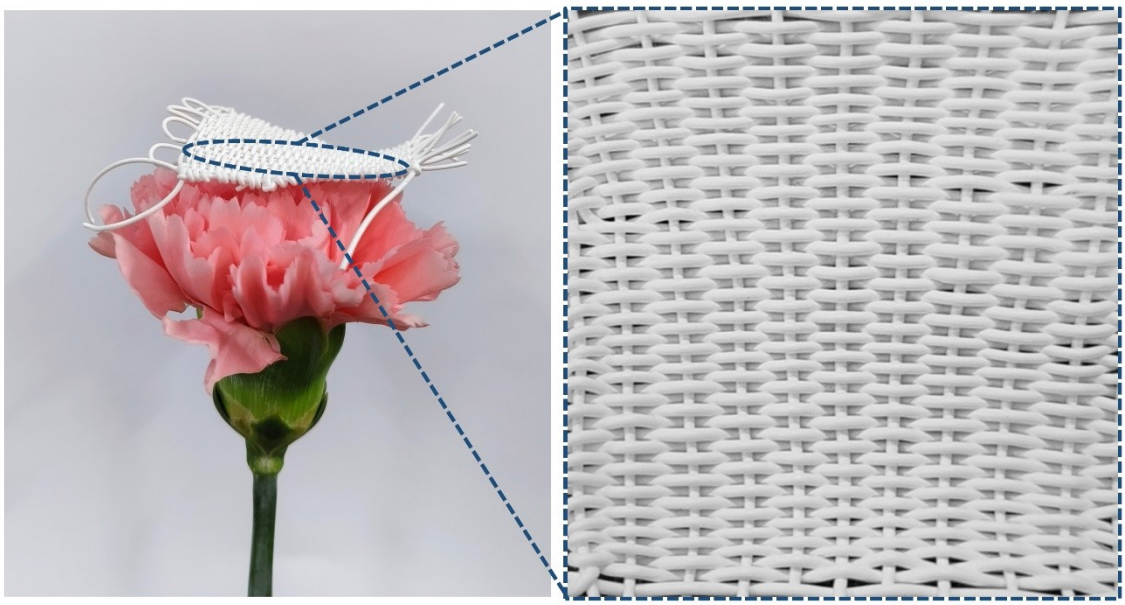

Fig. S23 The lightweight nature of the plain-woven fabric made by 20%TAF_{EtOH60}-APD and its enlarged structural diagram.

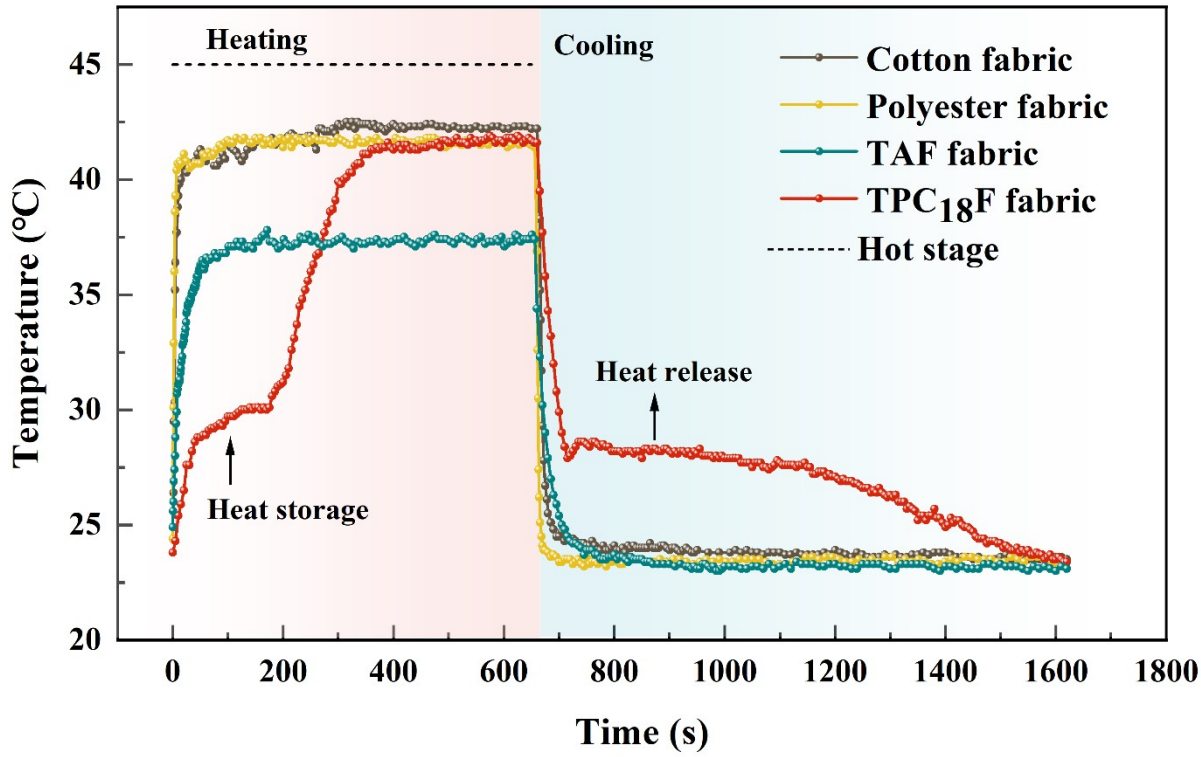

Fig. S24 Surface temperature variations of $TPC_{18}F$ fabric and TAF fabric as a function of time during the heating (45 ℃) and cooling process using cotton fabric and polyester fabric for comparison.

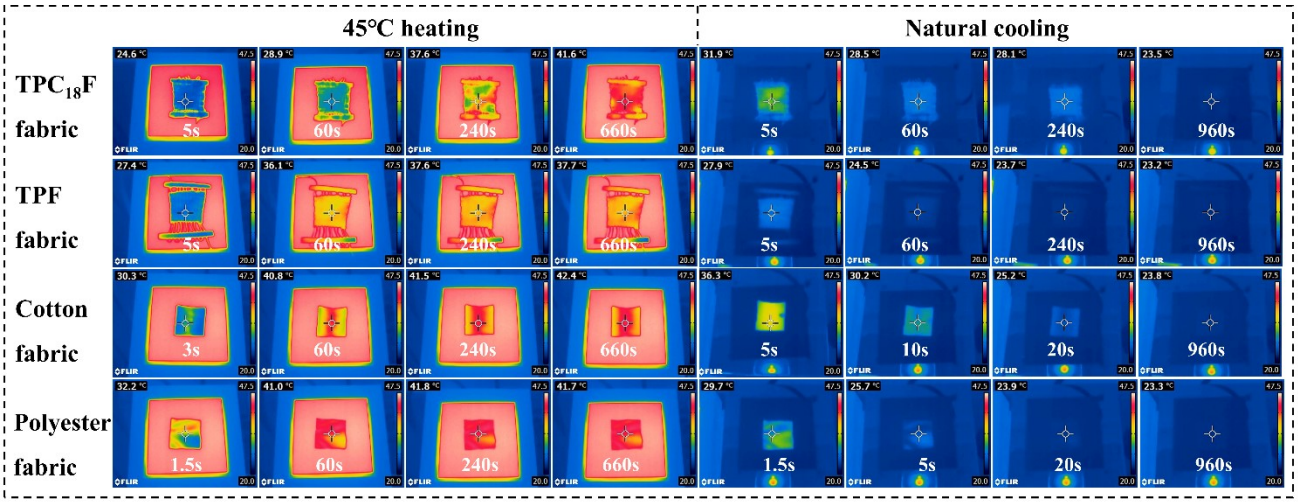

Fig. S25 Time sequential infrared images of $TPC_{18}F$ fabric, TAF fabric, cotton fabric and polyester fabric on a hot plate of 45 ℃ for heating and after reaching the maximum temperatures and on a cold

plate of 23.5 ℃ for natural cooling.

3. Supporting Table

Table S1. The parameters used in the Tyn-Calus formula to calculate the dynamic diffusion coefficients.

Solvents	V_A (cm^3/mol)	σ_A （dyn/cm）	V_B (cm^3/mol)	η_B （cP）	σ_B （dyn/cm）
DMF	77.38	36.44	/	/	/
DMSO	71.26	43.1	/	/	/
H_2O	/	/	18.08	0.8	72.81
Ethanol	/	/	58.27	1.09	22.87
Acetic acid	/	/	57.25	1.22	27.6
Isopropyl alcohol	/	/	76.56	2.04	21.7

* T = 303.15 K.

Table S2. The dynamic diffusion coefficients of solvent A into solvent B

Solvent B	$D_{DMF\text{-}in\text{-}B}$ (cm^2/s)	$D_{DMSO\text{-}in\text{-}B}$ (cm^2/s)
H_2O	1.237×10^{-5}	1.250×10^{-5}
Ethanol	1.043×10^{-5}	1.054×10^{-5}
Acetic acid	9.541×10^{-6}	9.642×10^{-6}
Isopropyl alcohol	5.948×10^{-6}	6.011×10^{-6}

Table S3. Comparison of TPU aerogel fibers formed with different spinning solution concentration under BSR-APD strategy.

TPU aerogel fibers	Density (g/cm^3)	Porosity (%)	Radial shrinkage (%)	Thermal conductivity of woven fabric (W/m·K)
15% TAF_{EtOH60}-APD	0.288	76.02	2.76	0.0479
20% TAF_{EtOH60}-APD	0.302	74.81	2.51	0.0486
25% TAF_{EtOH60}-APD	0.453	62.28	0.59	0.0498
30% TAF_{EtOH60}-APD	0.551	54.11	0.27	0.0501

Table S4. Comparison of the mechanical properties of TPU aerogel fibers and TPU phase change fibers.

Solvents	Samples	Tensile stress (MPa)	Elongation at break (%)
DSMO	20%$TAF_{DMSO\text{-}in\text{-}H_2O}$-APD	2.02	444.30
	20%$TAF_{DMSO\text{-}in\text{-}EtOH60}$-APD	2.72	514.69
DMF	20% TAF_{H_2O}-APD	2.92	614.46
	20% TAF_{AcOH60}-APD	3.17	500.98
	20% TAF_{IPA60}-APD	5.24	605.20
	20% TAF_{EtOH60}-APD	4.80	617.49
	20% TAF_{EtOH60}-FD	4.50	601.38
	25% TAF_{EtOH60}-APD	5.35	626.16
	30% TAF_{EtOH60}-APD	8.65	741.47
	20%$TPC_{18}F$-APD	5.25	635.35
	25%$TPC_{18}F$-APD	5.30	602.49
	30%$TPC_{18}F$-APD	5.48	639.03
	20%$TPC_{20}F$-APD	4.71	613.34
	20%$TPC_{22}F$-APD	4.94	616.53
	20%$TPC_{PEG}F$-APD	2.31	638.39

Table S4. Preparation and performances of recent reported phase change fibers.

Phase change fibers	Fiber matrix material	Phase change component	Preparation method	Breaking strength and Elongation at break	Elasticity	Phase Change Enthalpy	Ref
Phase Change Composite Fibers	PAN	PEG1000	coaxial wet spinning; vacuum impregnation	2.62 MPa, 13.86%	NA	128.6	[2]
SA-g-mPEG composite fibers	Sodium alginate	mPEG-NH_2	in-situ wet spinning	NA	NA	49.2	[3]
CNTs/SA-g-mPEG hybrid fibers	Sodium alginate	mPEG-NH_2	Graft; wet spinning	2.02 cN/dtex; 11.93%	NA	50.83	[4]
CuNPs/CS-g-mPEG hybrid fibers	Chitosan	mPEG	wet spinning	1.43 cN/dtex; 4.29%	NA	49.75	[5]
$fa_{2000}g_{2000}$-20	PA6	PTMEG	melt polymerization; melt spinning	2.12 cN/dtex; 80.21%	NA	12.44	[6]
TPF_1	TPU	PEG-ISA	coaxial wet spinning radical polymerization	3.8 MPa, 629.1%	NA	122.5	[7]
PU@OD4	TPU	OD	coaxial wet spinning	2.69 MPa, 370.07%	NA	160.14	[8]
T-12.5-1.5	TPU	OD	coaxial wet spinning	3.5 MPa, 623.9%	√	187.8	[9]
$TATF_{high\text{-}OD}$	TPU	OD	coaxial wet spinning	2.1 MPa, 710%	√	128.5	[10]
20%$TPC_{18}F$	TPU	C18	wet spinning;	5.25 MPa, 635.35%	√	193.2	**This work**

20%$TPC_{20}F$	TPU	C20	BSR-APD strategy; vacuum impregnation	4.71 MPa, 613.34%	√	182.3	**This work**
20%$TPC_{22}F$	TPU	C22		4.94 MPa, 616.53%	√	188	**This work**
20%$TPC_{PEG}F$	TPU	PEG1000		2.31 MPa, 638.39%	√	163	**This work**

Notes: PAN: polyacrylonitrile; PEG: polyethylene glycol; mPEG: Polyethylene glycol monomethyl ether; mPEG-NH_2: Amine terminated-polyethylene glycol monomethyl ether; SA: sodium alginate; PA 6: polyamide 6; PTMEG: polytetramethylene glycol; TPU: thermoplastic polyurethane; PEG-ISA: Acrylate-terminated PEG; OD: C18, octadecane; C20: eicosane; C22: docosane.

References

[1] Y. Zhu, M. Chen, J. Yan, R. Tan, C. Lin, S. Jiang, W. Wang, H. Xiao, E. Ren, H. Tang and R. Guo, *Compos. Part A-Appl. S.*, 2025, **193**, 108860.

[2] W. Mu, H. Cao, X. Cui, Z. Xu, T. Zhang and Y. Zhao, *ACS Appl. Polym. Mater.*, 2024, **6**, 15162–15171.

[3] S. Jia, D. Bao, N. Han, Z. Liu, J. Qiao, H. Zhang, J. Guo and S. Zhang, *J. Energy Storage*, 2024, **87,** 111411.

[4] J. Geng, S. Jia, D. Bao, D. Xiang, Y. shi, L. Liu, T. Zhang, J. Li, C. Tian, B. Zhou, H. Zhang, J. Guo and S. Zhang, *Int. J. Biol. Macromol.*, 2024, **282**, 137109.

[5] D. Bao, X. Zhang, X. Ji, Y. Xu, F. Guan, J. Guo and S. Zhang, *Int. J. Biol. Macromol.*, 2024, **281**, 135819.

[6] Y. Wu, S. Zhang, Y. Yu, C. Meng, R. Wang, C. Wang, H. Wang and P. Ji, *Chem. Eng. J.*, 2024, **500**, 157359.

[7] F. Xu, T. Zhang, Z. Xu and Y. Zhao, *J. Energy Storage* 2024, **79**, 110190.

[8] J. Zhang, Y. Zhang, S. Wu, Y. Ji, Z. Mao, D. Wang, Z. Xu, Q. Wei and Q. Feng, *Chem. Eng. J.*, 2024, **483**, 149281.

[9] H. Cao, Z. Xu, T. Zhang and Y. Zhao, *Chem. Eng. J.*, 2023, **478**, 147389.

[10] J. Sui, S. Jiang, J. Peng, Z. Kang and J. Fan, *Adv. Sci.*, 2025, **12**, 2412448.